Boundary mixing in Orkney Passage outflow

Kurt Polzin, Alberto C. Naveira Garabato, Einar P. Abrahamsen, Loïc Jullion, Michael P. Meredith

AGU PUBLICATIONS

JGR

Journal of Geophysical Research: Oceans

RESEARCH ARTICLE

10.1002/2014JC010099

Key Points:
- The Heywood control volume budget requires extremely vigorous diapycnal mixing
- We find large mixing regionally, but it is insufficient to close the budget
- We hypothesize that the budget is closed by boundary mixing

Correspondence to:
K. L. Polzin,
kpolzin@whoi.edu

Citation:
Polzin, K. L., A. C. N. Garabato, E. P. Abrahamsen, L. Jullion, and M. P. Meredith (2014), Boundary mixing in Orkney Passage outflow, *J. Geophys. Res. Oceans*, *119*, 8627–8645, doi:10.1002/2014JC010099.

Received 2 MAY 2014
Accepted 17 NOV 2014
Accepted article online 21 NOV 2014
Published online 16 DEC 2014

Boundary mixing in Orkney Passage outflow

K. L. Polzin[1], A. C. Naveira Garabato[2], E. P. Abrahamsen[3], L. Jullion[4], and M. P. Meredith[3,5]

[1]Department of Physical Oceanography, Woods Hole Oceanographic Institution, Woods Hole, Massachusetts, USA, [2]National Oceanography Centre, University of Southampton, Southampton, UK, [3]British Antarctic Survey, NERC, Cambridge, UK, [4]Geophysical Fluid Dynamics Institute, Florida State University, Tallahassee, Florida, USA, [5]Scottish Association of Marine Science, Oban, UK

Abstract One of the most remarkable features of contemporary oceanic climate change is the warming and contraction of Antarctic Bottom Water over much of global ocean abyss. These signatures represent changes in ventilation mediated by mixing and entrainment processes that may be location-specific. Here we use available data to document, as best possible, those mixing processes as Weddell Sea Deep and Bottom Waters flow along the South Orkney Plateau, exit the Weddell Sea via Orkney Passage and fill the abyssal Scotia Sea. First, we find that an abrupt transition in topography upstream of Orkney Passage delimits the extent of the coldest waters along the Plateau's flanks and may indicate a region of especially intense mixing. Second, we revisit a control volume budget by Heywood et al. (2002) for waters trapped within the Scotia Sea after entering through Orkney Passage. This budget requires extremely vigorous water mass transformations with a diapycnal transfer coefficient of $39(\pm 10)\times 10^{-4}$ m^2 s^{-1}. Evidence for such intense diapycnal mixing is not found in the abyssal Scotia Sea interior and, while we do find large rates of diapycnal mixing in conjunction with a downwelling Ekman layer on the western side of Orkney Passage, it is insufficient to close the budget. This leads us to hypothesize that the Heywood budget is closed by a boundary mixing process in which the Ekman layer associated with the Weddell Sea Deep Water boundary current experiences relatively large vertical scale overturning associated with tidal forcing along the southern boundary of the Scotia Sea.

1. Introduction

Antarctic Bottom Water (AABW) has undergone significant change in the past three decades. Outside of the Southern Ocean, AABW has experienced warming and a decrease in volume [*Purkey and Johnson*, 2010]. This warming is most notable in the Scotia Sea and the wider South Atlantic [*Johnson and Doney*, 2006; *Meredith et al.*, 2008]. Evidence has been provided for a freshening of the dense shelf waters contributing to AABW, potentially as a result of increased glacial melting around Antarctica [*Jacobs and Giulivi*, 2010; *Rye et al.*, 2014], and freshening of AABW in the deep ocean adjacent to Antarctica has also been documented [*Aoki et al.*, 2005; *Rintoul*, 2007; *Jullion et al.*, 2013]. While the signatures of warming and freshening are clear, the dynamical linkages between shelf waters and the abyss have not been elucidated. A major contribution to AABW comes from the Weddell Sea [*Gordon et al.*, 2001; *Naveira Garabato et al.*, 2002]. Within the Weddell Sea, the properties of Weddell Sea Deep and Bottom Waters (WSDW and WSBW, the regional varieties of AABW, defined in Table 1) were much more stable through the early 2000s [*Fahrbach et al.*, 2004, 2011], seemingly at odds with the warming of AABW measured downstream in the Scotia Sea and wider South Atlantic.

Possible explanations for this puzzling inconsistency have been based upon the apparent dominance of wind stress in modulating the strength of the Weddell Gyre [*Martinson and Iannuzzi*, 2003], and documented relationships between AABW properties in the Scotia Sea, variability in regional winds and variations in the strength of the Weddell Gyre [*Meredith et al.*, 2008; *Jullion et al.*, 2010; *Meredith et al.*, 2011b]. Direct evidence linking variability in the wind stress over the northern rim of the Weddell Gyre to AABW properties in the southern Scotia Sea on relatively short time scales of months is provided in *Jullion et al.* [2010] and *Meredith et al.* [2011b]. *Meredith et al.* [2011b] argue that these short time scales are characteristic of a *barotropic* response, and that the ensuing perturbations in the strength of the Ekman flow at the bottom boundary are sufficient to change the depths at which isopycnals intersect the South Scotia Ridge, thereby perturbing the properties of the WSDW overflowing into the Scotia Sea.

Table 1. Neutral Density (γ^n) and Potential Temperature (θ) Definitions for the Regional Varieties of AABW in the Weddell Sea[a]

Water Mass	γ^n (kg m^{-3})	θ (°C)
Weddell Sea Deep Water	28.26 → 28.40	0.0 → −0.7
Lower WSDW	> 28.31	−0.25 → −0.7
Weddell Sea Bottom Water	> 28.40	<−0.7

[a]Weddell Sea Deep Water (WSDW) with $\gamma^n \geq 28.31$ is too dense to escape through Georgia Passage and is trapped within the Scotia Sea (Figure 1). Thus this isopycnal serves as the upper surface of the *Heywood et al*. [2002] control volume budget, and distinguishes Upper from Lower WDSW.

A modified version of this hypothesis is discussed herein. Evidence is provided for dramatically enhanced boundary mixing and remarkably thick (O(500 m)) bottom boundary layers within the major WSDW outflow over the South Scotia Ridge. We note that Ekman flow on the steeply sloping South Scotia Ridge is in the downwelling sense, with a tendency to overturn isopycnals in the WSDW density range: increased barotropic transport in response to wind forcing implies increased bottom velocities, increased downslope Ekman transports, and increased diapycnal mixing. We also discuss the potential for flow upstream of Orkney Passage to be hydraulically controlled, with related intense diapycnal mixing in hydraulic jumps.

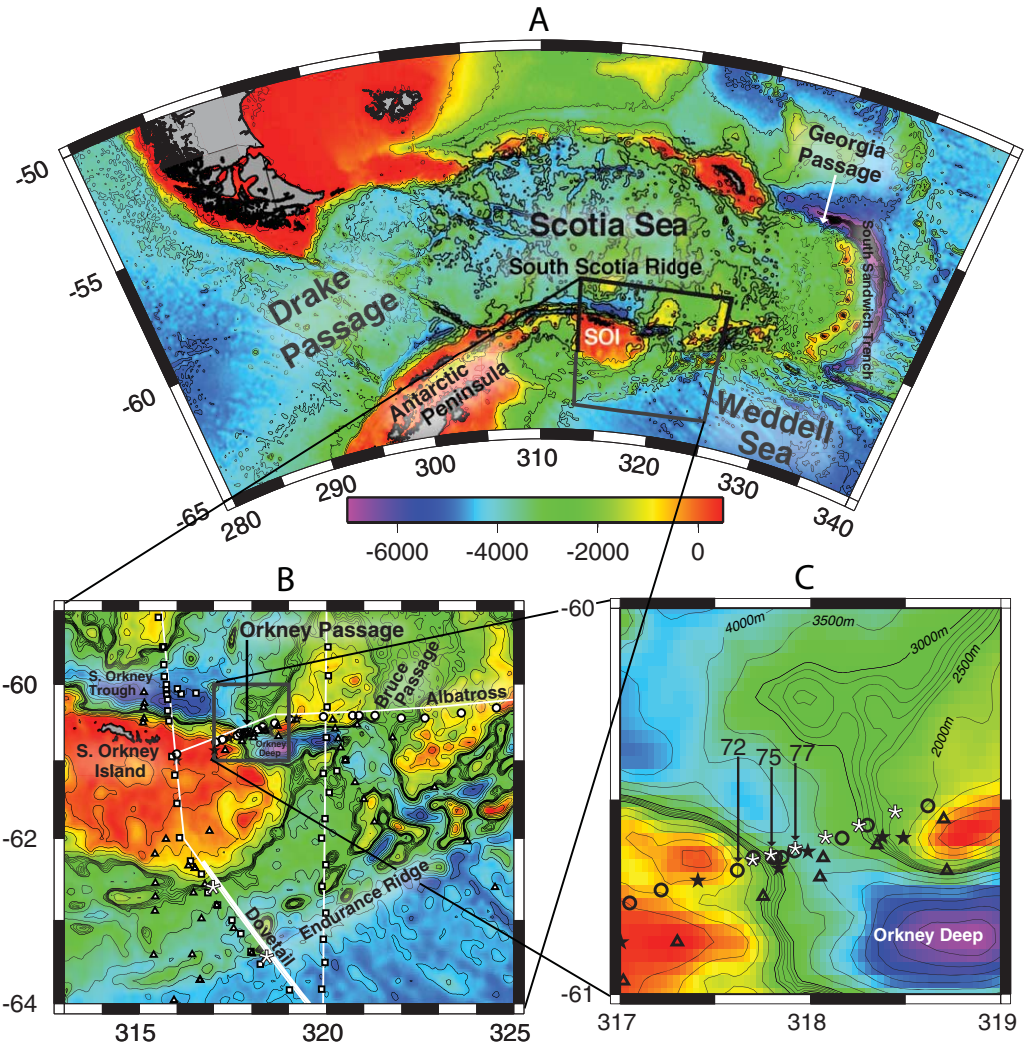

Figure 1. Place names and extant data. Bathymetry is from the Smith-Sandwell data set with contours every 500 m. Additional 100 m contours are used between 2500 and 3000 m water depth to emphasize topographic structure at depths slightly shallower than Orkney Passage sill depth. In Figures 1b and 1c, circles denote the location of station data obtained as part of ALBATROSS, squares DOVETAIL, triangles German/Brazilian CTD data, and stars German CTD/LADCP data. The DOVETAIL and ALBATROSS stations are highlighted with thin white lines and the DOVETAIL stations on the rise of the South Orkney Plateau are highlighted with a thick white line. The CORC-ARCHES and LTMS moored arrays are delineated by asterisks in Figures 1b and 1c, respectively. ALBATROSS stations 72 and 77 are designated in Figure 1c. See Figures 4 and 6 for details of the section (Stations 72–73-74–75-76–77) and Figures 3 and 5 for details of Station 75.

Our study achieves a quantitative focus with the *Heywood et al*. [2002] control volume study of Lower WSDW (Table 1), which uses Orkney Passage as a choke point and a bounding neutral density surface $\gamma^n = 28.31$ that grounds within the Scotia Sea. That study diagnoses significant diapycnal transformations in the southern Scotia Sea, characterized by an area-averaged diapycnal diffusivity $K_\rho = 39 \pm 10 \times 10^{-4}$ $m^2 s^{-1}$ derived from a temperature budget. Finescale parameterizations for diapycnal mixing driven by internal wave breaking are used to demonstrate that this mixing is unlikely to occur in the interior of the Scotia basin. Thorpe scale techniques are employed to document much more vigorous mixing in Orkney Passage, but such localized contributions do not appear sufficient to close the control volume budget. Even if extrapolated along the entire southern boundary of the Scotia Sea, such boundary mixing would only account for O(10%) of the diapycnal transformations required by the budget.

We therefore examine the assumptions of the *Heywood et al*. [2002] budget, yet are unable to offer a significant criticism that would lead to diapycnal transformations more than two standard deviations below the quoted uncertainty. Our leading hypothesis is to note that the slope of the southern boundary of the Scotia basin matches that of semidiurnal internal waves, and such critical conditions could, in combination with downwelling bottom Ekman layers, give rise to very large, transport-dependent diapycnal transformations that have yet to be documented.

Section 2 describes the data sets and methods employed in this study. Section 3.1 presents an interpretation of published analyses to motivate the current effort. Evidence for significant diapycnal mixing up and downstream of Orkney Passage is discussed in sections 3.2 and 4.2, with section 4.1 examining the dynamical processes manifest in individual stations in Orkney Passage. Possible interior and boundary contributions to the diapycnal transformations required by the *Heywood et al*. [2002] control volume budget are presented in sections 4.3 and 4.4. A summary and discussion is offered in section 5.

2. Methods

2.1. Data

We draw upon a broad collection of hydrographic and lowered acoustic Doppler current profiler (LADCP) data sets in our efforts to understand the transformation of WSDW and WSBW along the flanks of the South Orkney Plateau and within the Scotia Sea. These include three surveys with the context of documenting the ventilation of the Weddell Sea: the **D**eep **O**cean **Ve**ntilation **t**hrough **A**ntarctic **I**ntermediate **L**ayers (DOVETAIL) [*Gordon et al*., 2001], the **A**ntarctic **L**arge-Scale **B**ox **A**nalysis and **t**he **Ro**le of the **S**cotia **S**ea (ALBATROSS) [*Naveira Garabato et al*., 2002] and the **An**tarctic **D**eep Water **R**ates of **Ex**port (ANDREX) [*Jullion et al*., 2014] programs. The passage itself is a choke point and provides a unique opportunity to monitor climatic change in AABW, so the region has been instrumented with moorings at various times: south of Orkney Plateau (Figure 1b), as part of the NOAA **C**onsortium on the **O**cean's **R**ole in **C**limate – **A**b **R**upt climate **CH**ang **E** **S**tudies (CORC–ARCHES) program (led by A. Gordon and others at Lamont-Doherty Earth Observatory), and within Orkney Passage itself (Figure 1c), as part of the UK **L**ong **T**erm **M**onitoring and **S**urveying (LTMS) program (led by M. Meredith and others at the British Antarctic Survey (BAS), in collaboration with the NOAA Ocean Climate Observation Program (B. Huber and A. Gordon)). Regionally, there are two repeat hydrographic sections: the SR1b transect [*Meredith et al*., 2011a] across eastern Drake Passage, and the A23 transect [*Meredith et al*., 2013, and references therein] across the eastern Scotia Sea. ALBATROSS represents the 1999 occupation of A23. JR281 represents the 2013 occupation of SR1b and LTMS mooring turn around. Thus:

1. The intensity of turbulent diapycnal mixing within Orkney Passage proper is assessed using a Thorpe scale analysis [*Thorpe*, 1977] applied to six cross-passage transects. The ALBATROSS survey of the passage provides the impetus for this work and is complemented by the ANDREX survey [*Meredith*, 2010] and 4 BAS LTMS cruises (referred to as ES031 [*Nicholls et al*., 2007], ES033 [*Nicholls et al*., 2009], JR252 [*Abrahamsen*, 2011], and JR281 [*Sheen et al*., 2014]) conducted in conjunction with mooring operations.
2. The intensity of turbulent diapycnal mixing associated with turbulent production from internal wave breaking is assessed via the application of finescale parameterizations [*Polzin et al*., 2014]. The parameterization is applied to data from ALBATROSS (along A23), to DOVETAIL in the immediate vicinity of Orkney Passage and to the 1998 occupation of SR1b.

Table 2. Bandwidth Particulars for the Application of the Finescale Parameterization in this work[a]

Cruise	Stations	Lat S	Lon W	Shear (m^{-1})	Strain (m^{-1})
ALBATROSS	102–110	60.32–57.80	30.96–30.82	$\frac{1}{320}-\frac{2}{320}$	$\frac{1}{320}-\frac{2}{320}$
SR1b 1997	3–20, 23	61.05–58.84	55.96–54.61	$\frac{1}{320}-\frac{3^*}{320}$	$\frac{1}{320}-\frac{6}{320}$
DOVETAIL	7–16, 53–55	60.33–59.76	48.26–43.50	$\frac{1}{640}-\frac{2}{640}$	$\frac{1}{640}-\frac{6}{640}$

[a]The asterisk indicates reduced bandwidth at the two deepest transform intervals.

3. The measurements from two of the transects across Orkney Passage in which LADCP data quality and cross-passage spatial resolution are highest (ALBATROSS and JR281) are used to calculate volume transports of WSDW into the Scotia Sea.
4. The large-scale context of the AABW flow through Orkney Passage is investigated in section 3.2 by examination of five German and Brazilian-led transects in the northwestern Weddell Sea, discussed by *Schröder et al*. [2002]. One of these hydrographic surveys (AR XVIII) represents a contribution to DOVETAIL.

2.2. Finescale Parameterization of Diapycnal Mixing

The contribution of internal wave breaking to K_ρ in the far field of Orkney Passage is assessed using the finescale parameterization formula for turbulent production, $\mathcal{P}$ [*Polzin et al*., 2014, equation (40)], given by

$$\mathcal{P} = 8\times10^{-10}\frac{f}{f_o}\frac{N^2\cosh^{-1}(N/f)}{N_o^2\cosh^{-1}(N_o/f_o)}\hat{E}^2\,\frac{3(R_\omega+1)}{4R_\omega}\sqrt{\frac{2}{R_\omega-1}}. \quad (1)$$

The factor $\hat{E}$ represents a band-limited estimate of the shear spectral density relative to the high-wave number asymptote of the *Garrett and Munk* [1976] spectrum, $2\pi N^2/10$, and R_ω is the ratio of shear to strain spectral density. Shear is the gradient analogue of kinetic energy, and strain represents the rarification and compression of isopycnals as a gradient analogue of potential energy. The factor $\sqrt{\frac{2}{R_\omega-1}}$ is a single-frequency interpretation of the expected value of the aspect ratio, k_h/m, in a broadband wave field, in which k_h is the magnitude of the horizontal wave number and m is the vertical wave number. The factors $f_o = 2\pi\Omega\,|\sin(32.5^\circ \text{ latitude})|$ and $N_o = 3$ cph are normalization constants, with Ω equal to twice the Earth's rotation rate. The diapycnal buoyancy flux associated with this turbulent production is $R_f\mathcal{P}$, where the flux Richardson number $R_f \cong 0.15$.

An extensive review of this finescale parameterization is presented in *Polzin et al*. [2014], which documents the parameterization's use and its potential for bias. The most important of these relating to instrumental limitations is the bandwidth for estimating the spectral density. The bandwidth (Table 2) was chosen here on the basis of avoiding noise. No attempt was made to subtract noise or correct for suppression of oceanic signal by the data processing algorithms. Shear-strain ratios in the upper and lowermost two depth bins were respectively replaced with representative thermocline and abyssal values to avoid contamination of strain by nonwave density fine structure. Our analysis of the DOVETAIL data set relies on a strain-only algorithm below 3000 m, due to decreasing signal-to-noise ratios in the LADCP measurements. A significant physical limitation is that the finescale parameterization is a closure for wave-wave interactions. The associated downscale energy transfer can be dominated by wave-mean interactions when the Froude number $F_r = \bar{u}_z/N$ characterizing the background shear is larger than 1/8 [*Polzin et al*., 2014, section 2.3.4]. Significantly larger Froude numbers are found in the Orkney Passage, section 4.1, and thus we apply the parameterization only outside this domain.

2.3. Thorpe Scale Estimates of Diapycnal Mixing

An alternative to the finescale parameterization is the Thorpe scale method [*Thorpe*, 1977], which relates overturns at the outer scales of turbulence to the rate of dissipation of turbulent kinetic energy ϵ by molecular viscosity at subcentimeter scales [*Dillon*, 1982]. The Thorpe scale $L_T = (z'^2)^{1/2}$ represents the rms vertical displacement z' in an overturn resulting from sorting a density profile to be statically stable. The buoyancy flux is obtained via an empirical relation between the Thorpe scale and the Ozmidov length $L_o = (\epsilon/N^3)^{1/2}$, namely $L_o = cL_T$, where c is an $O(1)$ constant of proportionality (e.g., $L_T = 0.95L_o$) [*Ferron et al*., 1998]. The buoyancy flux $\mathcal{B}$ is thus

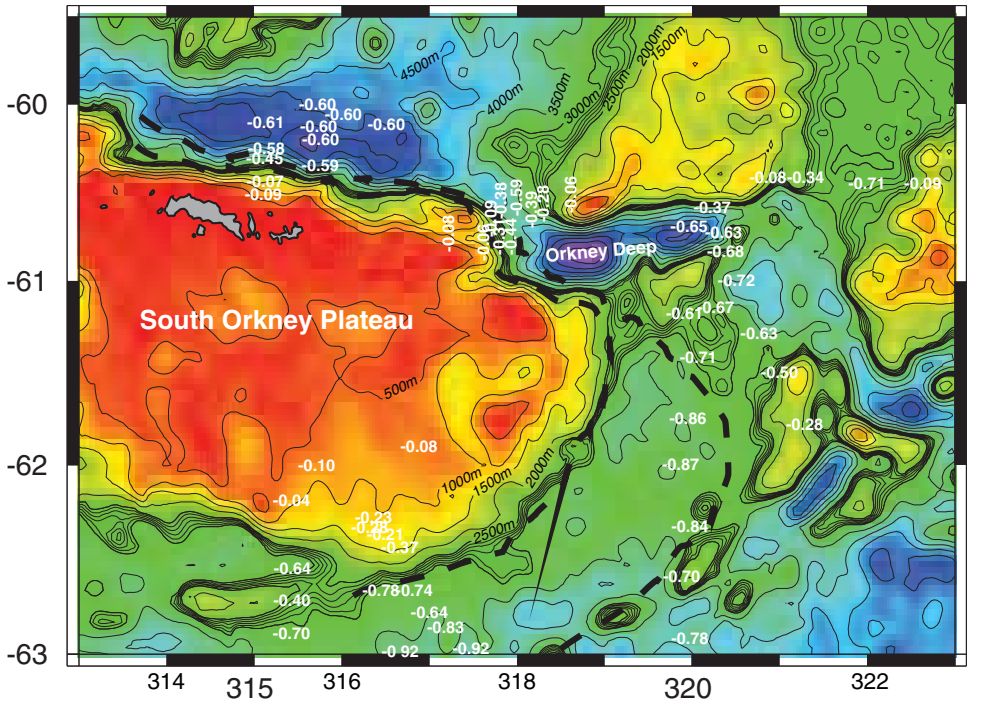

Figure 2. Bathymetry with bottom potential temperature measurements superimposed. Bathymetry is from the Smith and Sandwell data set with contours every 500 m. Additional 100 m contours are used between 2500 and 3000 m water depth to emphasize topographic structure at depths slightly shallower than Orkney Passage sill depth. Multibeam data taken in Orkney Passage environs add detail and confirm the relative depths of pathways into Orkney Deep, but does constrain the depth of the intervening saddle. Numbers posted in white represent bottom potential temperature values from hydrographic data. Dashed lines depict a hypothetical pathway for WSDW and WSBW through Orkney Passage.

$$\mathcal{B}=\Gamma\rho_o\epsilon=\Gamma\rho_o c^2 L_T^2 N^3. \tag{2}$$

The Ozmidov length, in turn, represents the vertical scale at which the inertial forces of turbulence balance buoyancy forces. Implicit is an assumption that the vertical scale is free to evolve so that this is possible. A note of caution is required here: within a boundary layer, the vertical overturning scale may be dictated by the boundary layer structure.

While relatively assumption-free in comparison to the finescale parameterization, the Thorpe scale method is best applied to density profiles obtained with specialized free-falling profilers rather than with wire-lowered instrumentation, as ship heave is communicated to the instrument package via the lowering wire, and may thereby trigger a number of CTD sensor response issues [*Polzin et al*., 2014, section 4.2.1]. Such contamination is most prominent at periods typifying ocean swell (about 10 s), which translates to 10 m vertical wavelengths at lowering rates of 1 m s^{-1}. There is a healthy discussion [e.g., *Gargett and Garner*, 2008, and references therein] on the inference of overturns in the presence of noise. The context in this work, though, is one of highly energetic turbulence with O(10–100 m) vertical scale overturns that minimizes such concerns. Here we estimate the Thorpe scale using 2 dbar pressure-binned CTD data and employ both neutral density and potential temperature to identify overturns. As a quality control measure, we require overturns to have a Thorpe scale in excess of 5 m, which translates into an overturn height of approximately $2L_T=10$ m, and avoids the worst of package motion contamination. This puts a resolution limit on the dissipation rate of approximately $\epsilon_{min}\cong(5\,\mathrm{m})^2(5.5\times10^{-4}\,\mathrm{s}^{-1})^3\cong5\times10^{-9}$ W/kg. This resolution limit precludes use of the Thorpe scale technique in the basin interior, which hosts abyssal dissipation rates one order of magnitude smaller (section 4.3). As a further quality control measure we also require a neutral density (potential temperature) anomaly three times larger than a lower bound, $\gamma^n_{rms}=(0.5-1.0)\times10^{-3}/3$ ($\theta_{rms}=1\times10^{-4}$C).

The buoyancy frequency N across the overturn is estimated in two ways: a finite difference version of the adiabatic leveling method [*Polzin et al*., 2014] using the CSIRO seawater routines and by least-squares

regression of the sorted γ^n profile. For the Lower WSDW layer, we find that $-\frac{g}{\rho_o}\frac{\partial\gamma^n}{\partial z} \cong 2N^2$, and use this approximate relation in the Thorpe scale calculations. See *Iudicone et al*. [2008] for further discussion of the regional neutral density definition.

3. Context

Here we set the stage by reviewing circulation and temperature distributions in the vicinity of Orkney Passage (Figure 2).

3.1. Circulation and Transport

Gordon et al. [2001] used LADCP measurements to quantify the absolute velocity field across the northern limb of the Weddell gyre, and estimated that some 12 Sv of newly ventilated WSDW and WSBW flow eastward along the South Orkney Plateau slope. They argued that these waters leave the Weddell Sea through gaps in the South Scotia Ridge, noting that WSBW ($\theta < -0.7$C) is not found to the north of the ridge. This led them to conjecture that intense mixing at an unresolved sill must be responsible for the absence of WSBW in the Scotia Sea. The DOVETAIL survey also documented a coarsely sampled 10 Sv *westward* transport of WSDW north of the South Orkney Plateau.

Naveira Garabato et al. [2002] similarly used LADCP measurements to assess the absolute velocity field during the ALBATROSS campaign in April 1999. That section transits along the South Scotia Ridge crest and crosses Orkney Passage, directly surveying the outflow into the Scotia Sea (Figure 1c). The northward transport of WSDW is evident as a bottom-intensified current on the western side of Orkney Passage, with a weak southward flow on the eastern flank of the gap. Transport through Orkney Passage dominates the total observed flux of WSDW over the South Scotia Ridge (6.0 $\pm$0.6 out of a total 6.7 $\pm$1.7 Sv). WSBW is found only within Bruce Passage, just to the east of Orkney Passage. The associated WSBW transport, however, is negligible, as is the WSDW transport (0.1 $\pm$1.2 Sv).

These two transport estimates are comparable to, but larger than, a third estimate provided herein (Section 4..2). *If* transport variability is linked both to the intensity of boundary mixing and to integrated measures of water mass conversion rates, then the temporally sparse available observations may introduce significant biases in our estimates of all three terms in (3). See Sections 4..2 and 5. for further discussion. We further note that DOVETAIL sampling on the steeply sloping flanks of the South Orkney Plateau is too coarse to extract meaningful Thorpe scale estimates of diapycnal mixing, and that casts from the ODCB data base appear to have had static instabilities removed from them, such that a Thorpe scale calculation is not viable.

3.2. Upstream Mixing?

A compelling feature of extant data sets is the spatial distribution of bottom potential temperature (Figure 2). Waters colder than -0.85°C were found on the southern flank of South Orkney Plateau, just upstream of Orkney and Bruce passages, in both 1998 [*Gordon et al*., 2001] and 2000 [*Schröder et al*., 2002]. Downstream of Orkney Passage, north of the South Scotia Ridge, the coldest bottom potential temperatures in DOVETAIL are -0.60°C or warmer, leading *Gordon et al*. [2001] to speculate that this lack of WSBW ($\theta < -0.7^\circ$C) might imply mixing at an unresolved sill. The ALBATROSS data from 1999 reveal a bottom potential temperature of -0.71°C in Bruce Passage, just to the east of Orkney Passage, but this has little transport associated with it [*Naveira Garabato et al*., 2002]. Data from Orkney Passage during ALBATROSS are warmer still ($\theta > -0.60^\circ$C) and subsequent CTD surveys (ANDREX and hitherto unpublished LTMS turnarounds) indicate the coldest water to have relatively stable temperatures, ranging from -0.59 to -0.63°C. This temperature difference (-0.85 to -0.63°C) exceeds the extremes of variability observed in a 4 year time series on the southern flank of South Orkney Plateau [*Gordon et al*., 2010], suggesting that either the [*Gordon et al*., 2001] DOVETAIL measurements to the south are highly anomalous or that a significant conversion of WSBW to WSDW must occur upstream of Orkney Passage.

The available data are insufficient to ascertain the fate of newly ventilated WSBW found on the southern flank of South Orkney Plateau. We think it likely that WSBW is increasingly trapped to a topographic boundary upstream of Orkney Deep (Figure 2, dashed lines), entering that deep basin over a $\sim$ 2500 m deep sill. The WSBW signature could be erased either as the inflow pitches over a steep (1:4) slope into Orkney Deep, or prior to that if flow is sufficiently enhanced along the boundary. An alternate passage into Orkney Deep exists to the east via a deeper ($\sim$ 3000 m) sill. Multibeam data (not shown) corroborate the relative

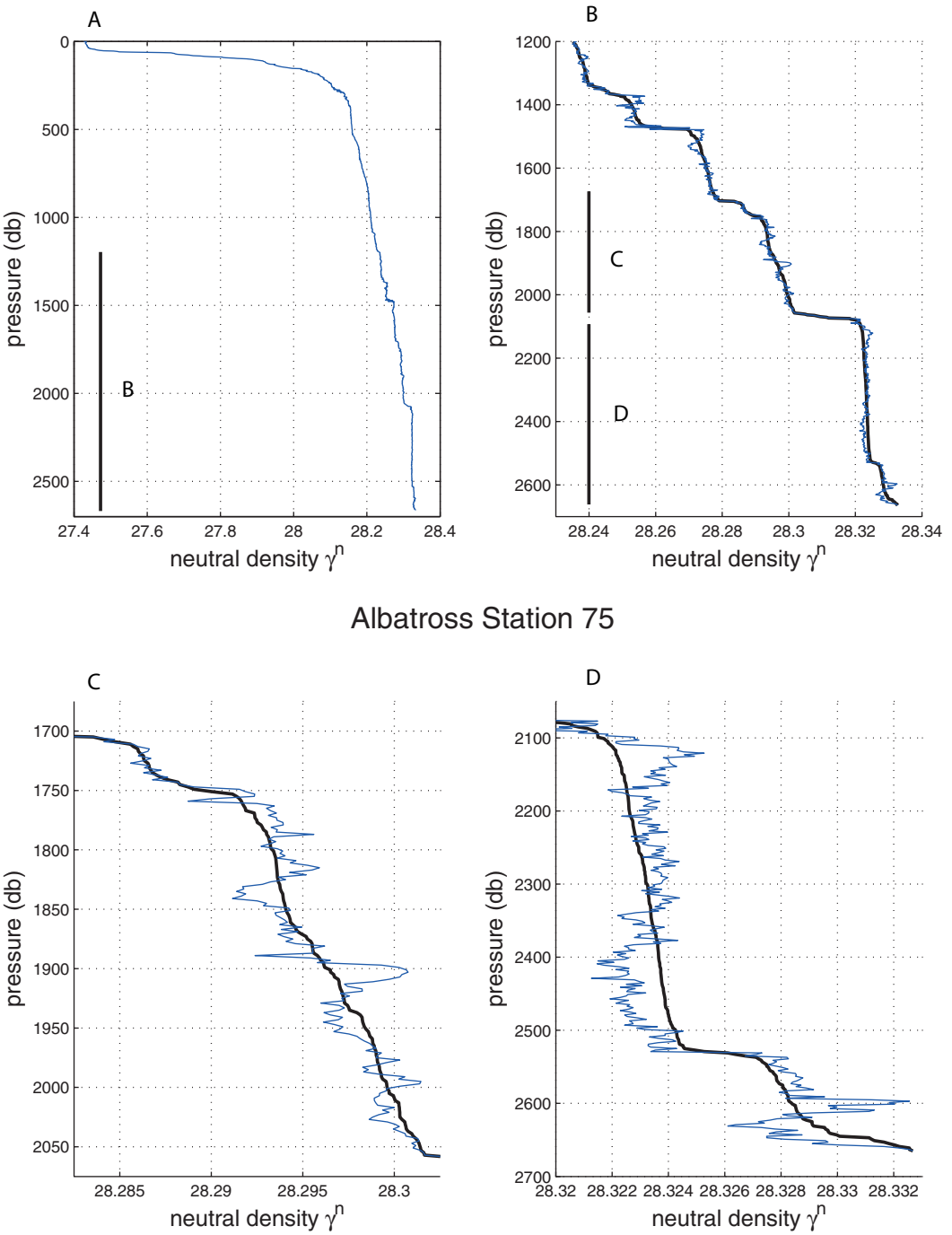

Figure 3. Neutral density profile for ALBATROSS station 75. The thin blue line represents the observed profile. Sorting the observed profile so that it is statically stable returns the thick black line. Figures 3b–3d are progressive enhancements of the total profile in Figure 3a. See Figure 5 for the corresponding velocity profile.

differences in sill height, but do not address the depth of an intervening saddle (Figure 2). Further survey work is required to document the pathway(s) of deep flow immediately upstream of Orkney Passage.

4. Evidence of Diapycnal Transformations

Qualitative evidence for diapycnal transformations within Orkney Passage is presented (section 4.1) before revisiting the control volume study of *Heywood et al*. [2002] (section 4.2). We thereafter assess the relative

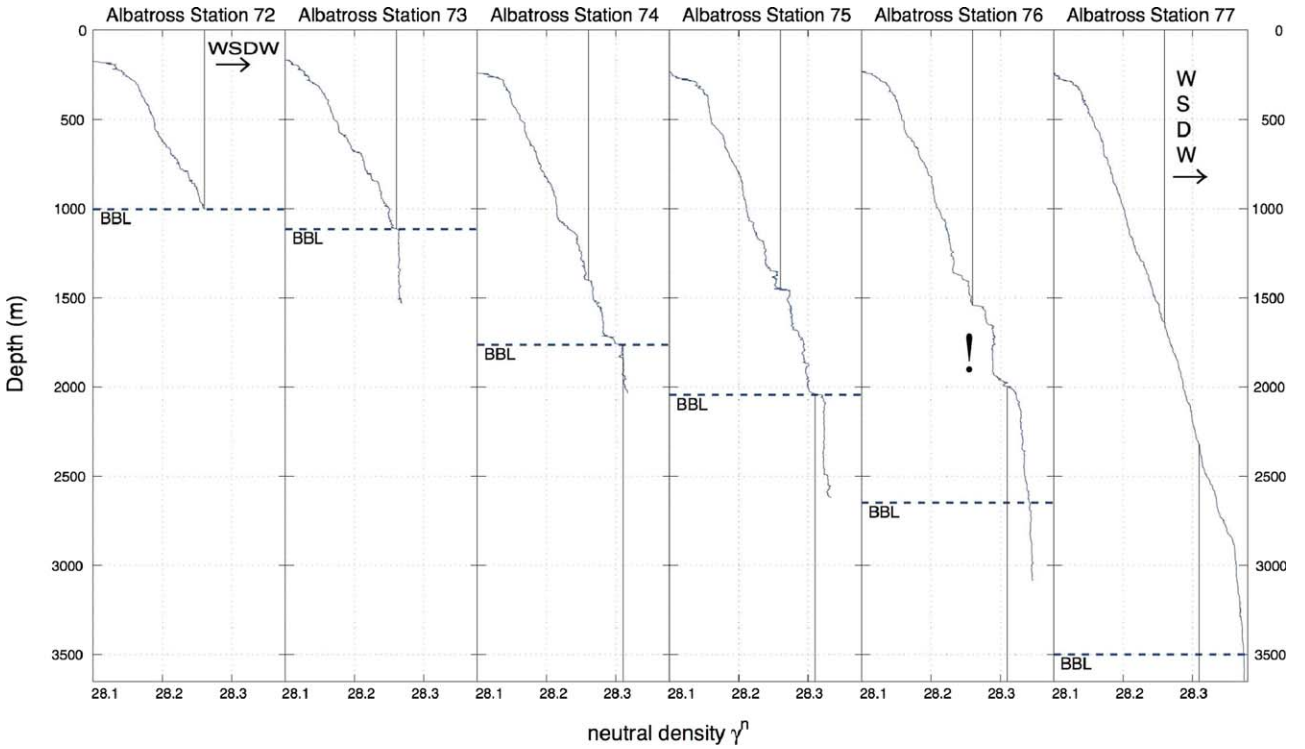

Figure 4. Neutral density profiles on the western side of Orkney Passage. The vertical lines demarcate the $\gamma^n = 28.26$ and $\gamma^n = 28.31$ kg m^{-3} isopycnal surfaces. The horizontal dashed lines represent the top of the bottom boundary layer. Note both a general tendency for reduced stratification at the western boundary, increased finescale variability and the 250–300 m high overturn centered at 1800 m in the station 76 profile. See Figure 6 for the corresponding velocity profiles.

roles of turbulent fluxes associated with 'interior' (Section 4..3) and 'boundary' (Section 4..4) diapycnal mixing in balancing the advection of temperature into the deep Scotia Sea via Orkney Passage.

4.1. Mixing Within Orkney Passage

Enhanced fine structure within the Orkney Passage system is apparent as obvious steppiness in the density profiles and overturns of tens to hundreds of meters (Figure 3). Though weakly stratified, these overturning structures have density signatures well above noise levels. Particularly dramatic is an overturning structure with a height exceeding 400 m at station 75 (Figure 3d). The overturns and steppy stratification are local features. The density profile of station 77, in the middle of Orkney Passage (Figure 1c), is relatively smooth (Figure 4) and characteristic of regions outside the passage. A region of reduced stratification occupies the near boundary region on the western side of the passage (Figure 4), indicating a tendency of isopycnals to dip downward into that boundary. This region is demarcated by horizontal dashed lines. Overturns in excess of 50–100 m characterize this bottom boundary region in stations 73–76. Inspection of the velocity profiles (Figures 5 and 6), suggests the following interpretation.

Above the middepth maximum in along-channel velocity, the velocity is strongly sheared. Froude numbers ($F_r = |\bar{u}_z|/N$) estimated from linear trends over 800 dbar at station 75 are approximately 0.25, and additional velocity fine structure is embedded within the profile. Similarly constructed Froude numbers for1500–2000 dbar at station 76 are larger, approximately 0.4. While not large enough to be directly responsible for producing the overturning structure through a linear shear instability (typically quoted as $F_r > 2\,[R_i \equiv N^2/(\bar{u}_z^2 + \bar{v}_z^2) < 1/4]$), such values of background shear strongly suggest that turbulent production is associated with wave-mean flow interactions rather than wave-wave interactions [*Polzin et al.*, 2014].

Below the middepth maximum in along-channel velocity, the large overturning structure at the bottom of station 75 appears to be associated with the boundary layer. Standard Ekman layer theory involves a balance between the Coriolis force and a vertical stress divergence. On a sloping boundary, several investigators have argued that across-slope buoyancy advection within the boundary layer can create horizontal density gradients that quash turbulent fluxes and reduce the steady state Ekman layer to a balance

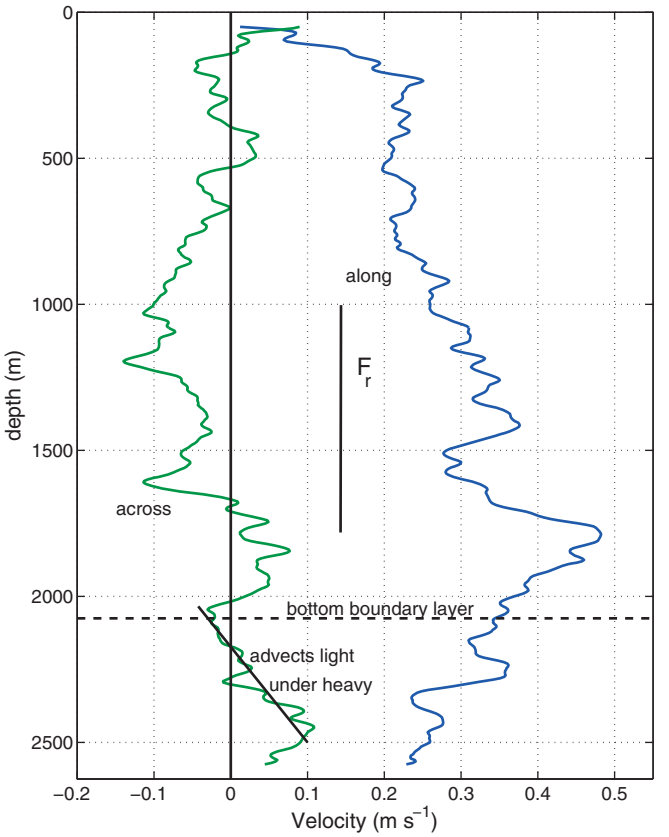

Figure 5. LADCP velocity profile for ALBATROSS station 75. Observed velocity components have been rotated into cross- (green) and along- (blue) slope coordinates. The along-slope velocity is strongly sheared above the middepth velocity maximum, with a Froude number of approximately 0.25 over the depth range of the shallow solid black line. The deep solid black line delineates the depth range over which downslope shear in the cross-slope velocity is found. The dashed line represents the nominal height of the bottom boundary layer. The vertical axis of the figure extends to the bottom boundary. See Figure 3 for the corresponding density profile.

between Coriolis force and pressure gradients [*Trowbridge and Lentz*, 1991; *MacCready and Rhines*, 1993; *Brink and Lentz*, 2010a]. Before a steady state is achieved, however, the cross-slope vertical shear in the Ekman layer can advect light water under dense and create statically unstable conditions. The observed cross-slope velocity profile at station 75 (Figure 5) indicates increasing downslope velocity with depth toward the bottom of the profile. Coupled with nearly vertical isopycnals associated with reduced near boundary stratification, Figure 4, such shear will advect lighter water under dense. The downslope velocity and large overturning structure (Figure 3d) are coincident in depth. Hence we interpret these features as associated with Ekman dynamics on a sloping boundary.

The overturning feature of station 75 indicates a boundary layer of surprisingly large vertical scale [$O \sim (500\text{m})$] that exceeds a standard Ekman depth scale [*Ralph and Niiler*, 1999] of $\sqrt{\tau/\rho f N} \cong 60\text{m}$, with bottom stress $\tau = \rho C_d U^2, C_d = 2-3\times10^{-3}$ and $U = 0.4$ m s^{-1}. A source of this discrepancy may lie in time-dependent contributions, e.g., tidal or eddy, unresolved by the individual stations. The topographic slopes along this flank of the South Orkney Plateau are steep, roughly $\frac{1}{4}-\frac{1}{5}$, and match the slope of semidiurnal internal wave trajectories of approximately σ/N, with $\sigma = \frac{2\pi}{12.4\,\text{h}}$ and buoyancy frequency estimated at equivalent depths from stations in midchannel ($N = 5.5\times10^{-4}$ s^{-1}). Thus this boundary layer may represent the superposition of two distinct phenomena: a downwelling Ekman layer [*Brink and Lentz*, 2010a], which sets up a nearly neutral stratification at the boundary and buoyancy gradients in the cross-slope direction, with differential cross-slope advection of density (documented in Figure 5) directly leading to overturning; and the amassing of ray characteristics associated with semidiurnal tides over a critical topographic slope [e.g., *Baines*, 1974], which will sustain cross-slope vertical shear and differential advection. A complicating factor is that, in contrast to the vertical scale being intrinsically tied to the Ekman dynamics of the time-dependent problem, as in *Brink and Lentz* [2010b], the vertical structure of the boundary layer may be externally imposed by the tidal shear for near-critical topography. Earlier studies [e.g., *Padman et al*., 2006] have shown this topographic region to be a site of M_2 internal tide generation. We therefore hypothesize that the interaction between the downwelling Ekman layer and the tidally generated cross-slope shear leads to overturns and enhanced mixing on the western flank of Orkney Passage.

While the flow field is highly sheared in the vertical, large horizontal velocity gradients are also inferred. First-difference estimates between station pairs return $R_o = \zeta/f \sim O(1)$. Despite such large spatial velocity

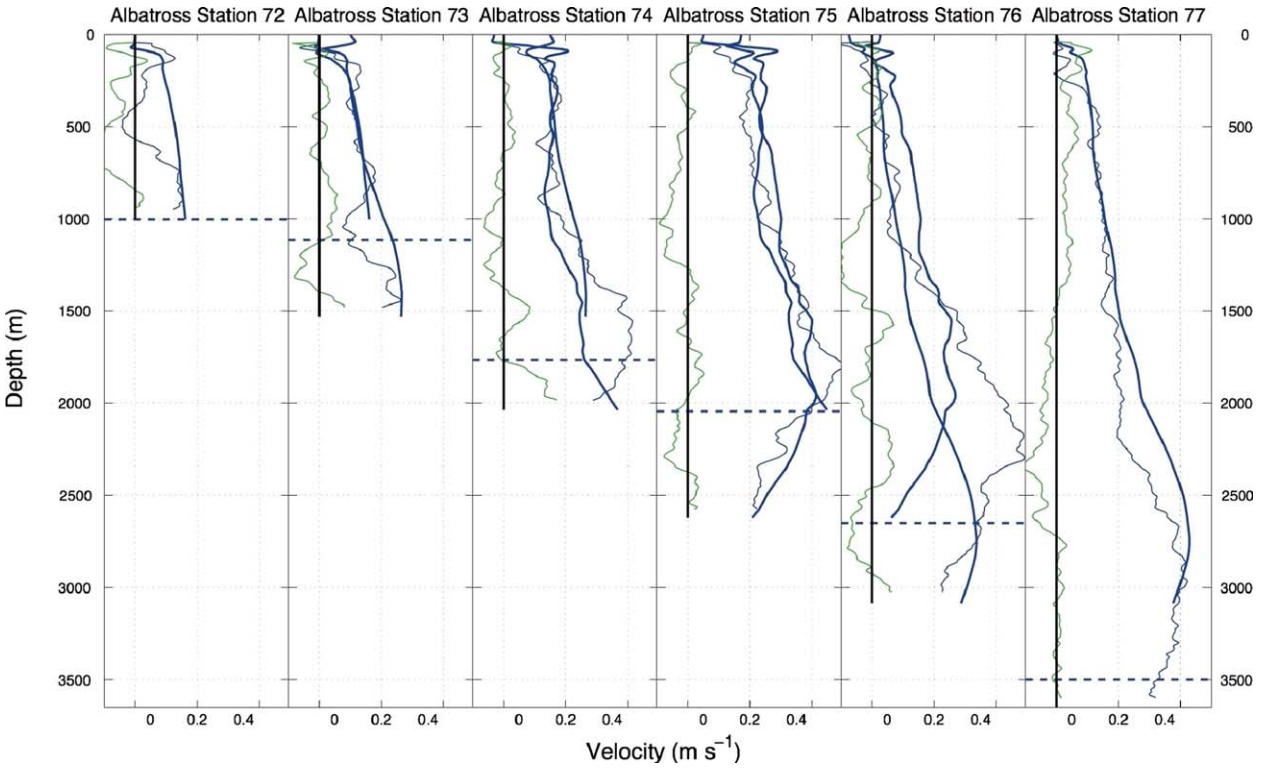

Figure 6. Velocity profiles on the western side of Orkney Passage. Observed velocity components have been rotated into cross- (green) and along- (blue) slope coordinates, and the ascending and descending traces averaged. The thick lines are geostrophic velocity estimates using the adjacent stations multiplied by a geometric factor to map the section normal geostrophic velocities into the along-slope velocity field. An offset has been added to produce a visual "best fit." The horizontal dashed line represents the top of the bottom boundary layer, based upon the detailed structure of the neutral density profile. See Figure 4 for the corresponding density profiles.

gradients, much of the observed large-scale structure in the velocity profile is crudely consistent with geostrophic estimates (Figure 6).

To summarize, inspection of the hydrographic and velocity measurements collected to date in Orkney Passage reveals that the passage outflow lies in an extreme dynamical regime characterized by high Rossby and Froude number ($R_o \sim 1, Fr \sim 1$) flow along topographic slopes that are critical with respect to semidiurnal internal wave trajectories. While the deepest layers of the outflow experience strong diapycnal upwelling immediately upstream of the passage, possibly as a result of downslope flow along the abrupt entry to Orkney Deep, elsewhere very intense boundary mixing appears to occur in association with downwelling Ekman flow on the passage's western slope. In the next section, we examine the relative importance of diapycnal mixing along boundaries within Orkney Passage and that in the interior of the Scotia Sea in closing the deep buoyancy budget of the basin, with a view to shedding light on the mechanisms controlling the evolution of the properties of the AABW exported from the Weddell Sea.

4.2. A Control Volume Budget of the Deep Scotia Sea

The mean diapycnal diffusivity averaged over the area spanned by the $\gamma^n = 28.31$ kg m^{-3} isopycnal in the Scotia Sea was estimated as $K_\rho = (39 \pm 10) \times 10^{-4}$ m^2 s^{-1} by *Heywood et al*. [2002] based on a control volume budget, which for potential temperature takes the form (A12):

$$K_\rho \cong T^i \frac{\theta^\gamma - \theta^i}{A\theta_z^\gamma}, \tag{3}$$

in which T^i is the volume transport at Orkney Passage, θ^γ is the volume weighted transport on an upper bounding neutral surface, elected here to be the Lower WSDW boundary, θ^i the volume weighted transport into the control volume at Orkney Passage, θ_z^γ the mean potential temperature gradient on the upper

Table 3. Control Volume Particulars[a]

	Heywood et al. [2002]	1999 LADCP	2013 LADCP
T^i/m^3 s^{-1}	$4.0 \pm 0.5 \times 10^6$	5.2×10^6	2.2×10^6
θ^i/°C	-0.438 ± 0.007	-0.470	-0.467
θ^γ/°C	-0.250 ± 0.003		
S^i	34.654 ± 0.002		
S^γ	34.663 ± 0.003		
A/m^2	$(7.0 \pm 1.0) \times 10^{11})$	1×10^{12}	
θ^γ_z/°C m^{-1}	$(2.7 \pm 0.3) \times 10^{-4}$		
S^γ_z/m^{-1}	$(6.8 \pm 0.5) \times 10^{-6}$		
K_ρ/m^{2}s^{-1}	$39 \pm 10 \times 10^{-4}$		
α^γ/°C^{-1}		1.3159×10^{-4}	
β^γ		7.5142×10^{-4}	
θ_y/° C m^{-1}		7.9×10^{-8}	4.1×10^{-8}
P_y/dbar m^{-1}		2.1×10^{-3}	2.5×10^{-3}
$K_\parallel$/m^{2}s^{-1}		3000	
C_b		2.82×10^{-8}	
T_b		1.12×10^{-5}	

[a]The second column contains geostrophic transport estimates by *Heywood et al.* [2002] and associated parameters for the Lower WSDW control volume. The third column revisits the *Heywood et al*. [2002] transport estimates using the direct LADCP velocity estimates, and the fourth presents a new direct transport estimate using data from JR281. Meridional gradients of pressure and potential temperature on the $\gamma^n = 28.31$ kg m^{-3} isopycnal represent linear regressions to data from the SR1b and A23 hydrographic lines in the western and eastern Scotia Sea, with quoted values indicating the average of the two regressions.

boundary, and A and area of that surface in the interior basin. Approximations required to arrive at (3) are discussed in Appendix A.

Our reassessment of this calculation indicates that this large value is robust, the only possible minor issue being the estimation of the area A using a coarse-resolution climatological data set. Inspection of *Heywood et al*. [2002, Figure 2] suggests that the area occupied by the $\gamma^n = 28.31$ kg m^{-3} surface does not extend to the Shackleton Ridge, whereas *Jullion et al*. [2013] find that this surface exists on all occupations of the SR1b section. We estimate the potential low bias of A as being roughly 30% for the data set used by *Heywood et al*. [2002].

There are a number of methods for estimating the volume transport, T^i, and associated potential temperature transports (A11) with the ALBATROSS data set. The value quoted by *Heywood et al*. [2002], $T^i = 4.0$ Sv (Table 3), corresponds to geostrophic velocities rendered absolute by reference to the station pair-averaged LADCP velocity profiles. One can also estimate the volume transport from the individual LADCP velocity profiles, which yields $T^i = 5.2$ Sv. Differences in these transport estimates are perceived to be largely associated with the treatment of bottom triangles and pronounced finescale variability in the LADCP data. The transport-weighted potential temperature flux, θ^i, decreases by a similar amount when using the LADCP velocities directly rather than the geostrophic velocities.

The *Heywood et al*. [2002] budget assumes that θ^γ is given by the area-averaged potential temperature on the bounding neutral density surface, implicitly presuming that upwelling is uniformly distributed over the Scotia basin interior. This assumption introduces an $O(10\%)$ potential bias into the results, as water on the $\gamma^n = 28.31$ kg m^{-3} isopycnal tends to be warmer and saltier toward the north.

The last parameter in (3) concerns the diapycnal gradient of potential temperature. The value of θ_z is representative of the abyssal stratification. Using *Heywood et al*.'s θ^γ_z and S^γ_z, we find that $N^2 = \alpha\theta^\gamma_z + \beta S^\gamma_z = 3.0 \times 10^{-7}$ s^{-2}, which compares well with interior stratification profiles in Figure 7.

The diapycnal velocity associated with isopycnal stirring and nonlinearity in the equation of state is

$$w^* \cong -\frac{gK_\parallel}{N^2}\left(C_b\theta^\gamma_y P^\gamma_y\right) = -3.5 \times 10^5 \text{ m}^2\text{ s}^{-1} \cong O(10\%T^i). \quad (4)$$

Information regarding the isopycnal stirring coefficient $K_\parallel$ is limited to a mixing length-based estimate in *Naveira Garabato et al*. [2011]. Those authors present estimates of $c_e K_\parallel$ in their Figure 5g, where c_e represents the correlation between eddy velocity and eddy potential temperature anomaly in the mixing length parameterization of the potential temperature flux. Averaging these estimates yields $K_\parallel \cong 3000$ m^2 s^{-1} with $c_e = 0.15$ [*Naveira Garabato et al*., 2014]. Upstream of Drake Passage, *Tulloch et al*. [2014] provide a model based isopycnal stirring coefficient of 500–1000 m^2 s^{-1} at depths greater than 2500 m. With $K_\parallel = 3000$ m^2 s^{-1}, the contribution of isopycnal stirring amounts to O(10%) of the advective residual. Thus, the eddy-induced downwelling associated with cabbeling is nontrivial, yet not a leading-order process. The estimates of meridional potential temperature gradient on the neutral density surface (Table 3) constrain variability in the approximation (A11) to O(10%).

A further clue regarding the magnitude of the diapycnal transformations is that the volume occupied by Lower WSDW (Table 1) along the SR1b transect exhibits a decreasing trend with marked variability on

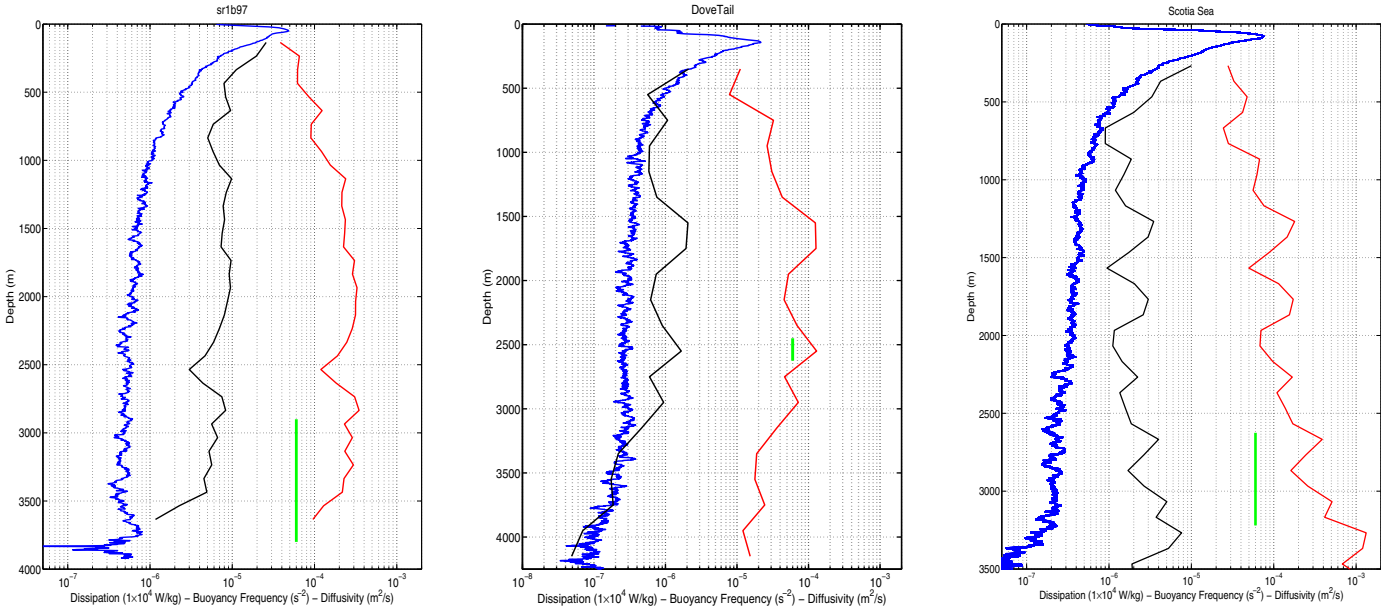

Figure 7. Fine structure parameterization based estimates for the dissipation rate and diffusivity. (left) the 1997 occupation of SR1b. (middle) DOVETAIL. (right) the eastern Scotia Sea segment of ALBATROSS. See Table 2 for station particulars. Black curves represent dissipation ϵ times 10^4, blue N^2 and red $K_\rho = 0.2\epsilon/N^2$. The vertical extent of the green line indicates the depth interval over which $\gamma = 28.31$ kg m^{-3} is encountered in the station. The $\gamma = 28.31$ kg m^{-3} horizon avoids regions of weak stratification in a trench at the base of the South Scotia Ridge and localized depressions in the eastern Scotia Sea. These weakly stratified regions have low signal-to-noise ratios in the LADCP and have been omitted from the figures.

periods of 3–5 years (E. P. Abrahamsen *et al*., in preparation). This area represents only the upper part of the control volume, and so is likely to undergo more significant oscillations in response to variations in transport at the inlet than is the entire control volume, $V = 3.0 \pm 0.5 \times 10^{14}$ m^3, for which *Heywood et al*. [2002] estimate a residence time of $V/T^i \cong 2.4$ years. Crudely, the Lower WSDW volume represents an average height of $V/A \cong 400$ m, whereas the thickness along the SR1b transect in 1998 is approximately 200 m. That the volume of lower WSDW on the SR1b line oscillates on time scale shorter than decadal suggests that the damping (mixing) time scale is *O*(years) rather than *O*(decades).

Finally, one additional transport estimate is possible with the JR281 data set obtained in 2013. This yields a direct (i.e., LADCP-based) volume transport of $T^i = 2.2$ Sv, and a transport-weighted potential temperature of $\theta^i = -0.467^\circ$C, see Table 3. This transport estimate is notably smaller than those obtained over a decade earlier during DOVETAIL and ALBATROSS, and raises the question of whether the differences are associated with either a trend or stochastic variability. Regardless, a volume transport of 2.2 Sv still requires large diapycnal transformations to occur downstream of the Orkney Passage sill. Similarly, while the biases that we report are potentially larger than *Heywood et al*.'s estimates of statistical uncertainty, their control volume budget appears to be sensibly robust, so we next consider where and how the implied very intense diapycnal mixing happens.

4.3. Mixing in the Basin Interior

Estimates of diapycnal mixing rates were obtained through the application of the finescale parameterization (1) to LADCP and CTD data from three cruises of the same approximate vintage as the *Heywood et al*. [2002] control volume budget: DOVETAIL, ALBATROSS, and the 1998 occupation of the SR1b section. These data were discussed in *Naveira Garabato et al*. [2004] as part of a study with a broader scope. Here we present averaged profiles for stations containing the $\gamma = 28.31$ kg m^{-3} density surface (Figure 7), which characterize turbulent mixing in the basin interior.

Diapycnal diffusivities and turbulent dissipation rates on the $\gamma = 28.31$ kg m^{-3} density surface in the basin interior are found to be one order of magnitude smaller than the basin-averaged values from the *Heywood et al*. [2002] control volume budget. Comparisons between finescale estimates and microstructure measurements made of mixing and dissipation rates conducted as part of the DIMES [*Sheen et al*., 2013] and SOFine

[*Waterman et al*., 2014] programs suggest a regional tendency for the fine structure parameterization to *overestimate* K_ρ. This reinforces the disparity between the fine structure-derived estimates and *Heywood et al*.'s control volume result. On a similar note, Sheen et al. [2014] discuss finescale observations from the SR1b section and present evidence of interannual variability of parameterized mixing tied to eddy activity and wind forcing in the northern and central sections of the Scotia Sea, with limited variability to the south.

Given the evidence of limited temporal variability of diapycnal mixing and a tendency of (1) to overestimate mixing rates in the region, we are led to infer that the mixing required by the *Heywood et al*. [2002] budget is *not* to be found in the interior of the Scotia Sea.

4.4. Boundary Mixing

The finescale parameterization (1) is a closure for the downscale cascade of energy associated with nonlinear internal wave interactions. In a highly sheared flow regime such as that in Orkney Passage, wave-mean interactions can dominate the downscale transports of energy that the parameterization [*Polzin et al*., 2014] attempts to capture. The finescale parameterization is also not intended to represent dissipation associated with boundary layers. We thus turn to a Thorpe scale analysis for mixing diagnostics.

Thorpe scale estimates of the turbulent buoyancy flux were made using station data from six occupations of Orkney Passage (Table 4 and Figure 8). Overturns were identified, and the rms overturning scale L_T was estimated using both neutral density and potential temperature. The buoyancy frequency N was estimated over slightly larger scales using both the adiabatic leveling method and the sorted neutral density profile (see Section 2..3 for details). The different methods provide section-average estimates of the buoyancy flux that differ by less than 50%. Variability is related to the potential temperature diagnostics providing fractionally larger estimates of overturning height, and to the neutral density-based estimates of N at the bottom boundary being occasionally larger. A relatively conservative approach to contamination of the density profile was taken by rejecting overturns with Thorpe scales smaller than 5 m. This requires an overturn height greater than about 10 m.

The Thorpe scale analysis clearly and consistently demonstrates enhanced mixing on the western side of Orkney Passage in conjunction with the outflow. Values of the buoyancy flux in excess of 1×10^{-7} W kg^{-1} apparent in the ALBATROSS occupation are more than two orders of magnitude larger than the *interior* values required to balance the *Heywood et al*. [2002] control volume budget. Yet considerable temporal variability is apparent, and the most intense mixing is limited to a short segment of steeply sloping topography.

To connect with the control volume we note that the *Heywood et al*. [2002] estimate of a diapycnal mixing coefficient implies an area-integrated buoyancy flux $\mathcal{B}$ of

$$\oint^{\gamma} \mathcal{B}\, dA \cong \rho_o K_\rho N^2 A \cong 9\times10^5 \text{kg m s}^{-3}. \tag{5}$$

Using the empirical relation between Ozmidov length and Thorpe scale, $L_o = cL_T$ (with $c = 0.95$ from *Ferron et al*. [1998]), the buoyancy flux $\mathcal{B} = \rho_o \Gamma c^2 N^3 L_T^2$, so that after integrating in the across-slope direction, the Thorpe scale analysis yields

$$\begin{aligned} \oint \mathcal{B}\, dA &\cong \int dx \left(\int dy\, \rho_o \Gamma c^2 N^3 L_T^2 \right) \\ &\cong L_x \tilde{\mathcal{B}}, \end{aligned} \tag{6}$$

where y is taken to be the cross-channel distance, x is the along-channel distance, and $\tilde{\mathcal{B}}$ is the result of averaging the Thorpe scale-derived buoyancy flux over a neutral density window of $\gamma^n = 28.31 \pm 0.02$ kg m^{-3} and integrating across the channel. The last line characterizes the area-integrated buoyancy flux as the product of $\tilde{\mathcal{B}}$ and a characteristic along-channel distance. See Table 4 for section-integrated estimates of the buoyancy flux.

While there is variability between occupations of Orkney Passage, the message is clear: the average Thorpe scale-derived estimate suggests that boundary mixing contributes $O(10\%)$ to the *Heywood et al*. control volume budget, if the near-boundary numbers in Orkney Passage can be extrapolated along the southern boundary of the South Scotia Sea, from Orkney Passage to the Shackleton Ridge, a distance of

Table 4. Estimates of Diapycnal Mixing From Thorpe Scales[a]

Cruise Data Set		$\tilde{\mathcal{B}}$ Via γ^n	L_x	$\tilde{\mathcal{B}}$ Via θ	L_x
ALBATROSS	April 1999	2.4e-01	4.1	2.6e-01	3.8
ES031	February 2007	2.7e-02	37	2.6e-02	38
ES033	February–March 2009	4.7e-02	21	5.9e-02	17
JR239 (ANDREX)	March–April 2010	2.5e-02	40	2.8e-02	35
JR252	March 2011	4.4e-02	22	6.1e-02	16
JR281	March–April 2013	1.9e-02	52	1.9e-02	52

[a]The tabulated values of L_x represent the distance required for closure of the *Heywood et al.* [2002] budget, i.e., 9×10^5 kg m^{-1} s$^{-3}/\tilde{\mathcal{B}}$, in multiples of 850 km, which is the distance along the southern boundary of the South Scotia Sea (from Orkney Passage to the Shackleton Ridge).

approximately 850 km. A typical value of $\mathcal{B}/\rho_o = 2\times10^{-8}$ W kg^{-1} over a cross-slope distance of 5 km and an along-slope distance of 1000 km returns an area-integrated buoyancy flux of $O(10^5)$ kg m s^{-3}, not the $O(10^6)$ kg m s^{-3} required by the control volume budget. Unfortunately, limited resources negate further

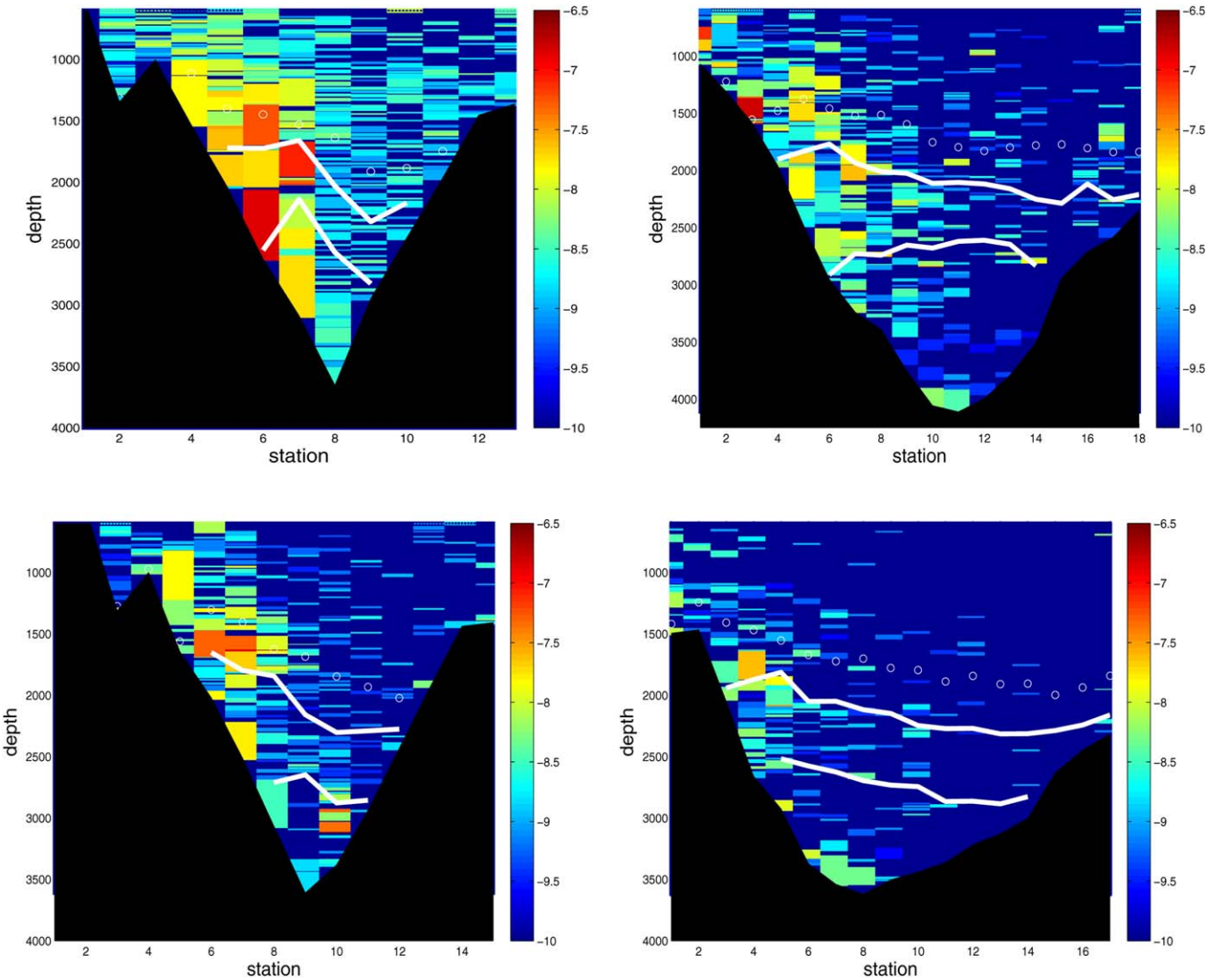

Figure 8. Buoyancy flux estimates $\mathcal{B}/\rho_o$ from a Thorpe scale analysis of four transects across Orkney Passage. Clockwise from top left: ALBATROSS, ES033, JR281 and ANDREX. White circles depict the first encounter of the WSDW upper boundary, $\gamma^n = 28.26$ kg m^{-3}, and the thick white lines represent $\gamma^n = 28.31 \pm 0.02$ kg m^{-3}. The color scheme is logarithmic with units of W kg^{-1}. The ES031 and JR252 occupations of Orkney Passage have significantly fewer stations and are not shown. The station spacing is highly nonuniform with steeply sloped pitches typically having greater mixing but representing smaller lateral extent. See Table 4 for the cross-slope integrated buoyancy flux estimates of all six sections.

investigation. DOVETAIL sampling on the steeply sloping flanks of the South Orkney Plateau is too coarse to extract meaningful Thorpe scale estimates of diapycnal mixing and casts from the ODCB data base appear to have had static instabilities removed from them, such that a Thorpe scale calculation is not viable.

5. Summary and Discussion

The rate and mechanisms of diapycnal water mass transformations in the Orkney Passage environs, and their standing in the buoyancy budget of the AABW in the abyssal Scotia Sea, are examined in this work, using data from multiple historical surveys of the regional hydrographic and velocity fields. A reassessment of the control volume study of *Heywood et al*. [2002] supports their conclusion that Lower WSDW experiences very large diapycnal transformations in the Scotia Sea after flowing over the Orkney Passage sill. These transformations are shown to not occur in the basin interior by a fine structure analysis of hydrographic and velocity data. Evidence of very intense turbulent dissipation and diapycnal mixing, respectively characterized by rates of 1×10^{-7} W/kg and 600×10^{-4} m^2 s^{-1}, *is* found in the Passage from a Thorpe scale analysis. However, extrapolation of the high rates of mixing estimated in Orkney Passage along the entire southern boundary of the Scotia Sea is found to account for only O(10%) of the basin-integrated buoyancy flux required by the control volume budget. We are thus unable to balance the *Heywood et al*. [2002] budget. We close by considering various hypotheses to resolve this tension.

Our leading hypothesis is that the budget is closed by boundary mixing along the southern boundary of the Scotia Sea. The western side of Orkney Passage hosts a downwelling bottom Ekman layer, associated with the WSDW outflow, that leads to nearly neutral stratification and pronounced cross-slope buoyancy gradients. Differential cross-slope advection of density (Figure 5) results in intense diapycnal overturning and mixing. This phenomenon is likely exacerbated by the criticality of the topographic slopes of the passage's western flank and southern Scotia Sea (typically $\frac{1}{4}-\frac{1}{5}$) to the semidiurnal internal tide [e.g., *Baines*, 1974], as previous studies [e.g., *Padman et al*., 2006] have shown the southern boundary downstream of the Passage to be a site of marked generation of M_2 internal tides. There is presently insufficient evidence to assess the extent to which this Ekman and tidal-related mixing occurs downstream of Orkney Passage. However, a high-ranking role of the boundary mechanism is consistent with the "wind control" hypothesis that *Meredith et al*. [2011b] put forward to explain the dependence of WSDW properties in the Scotia Sea on wind forcing of the northern Weddell gyre, reliant on the coupling between WSDW outflow transport and diapycnal mixing in Orkney Passage via bottom Ekman flows. Multiple mechanisms may provide a link between transport and mixing, as intense mixing in association with the plunging of AABW into the 6000 m deep Orkney Deep (Figure 2) is indicated by the range of bottom potential temperatures found within and immediately downstream of Orkney Passage (-0.63 to -0.58°C), which is both substantially warmer than bottom potential temperatures of -0.85°C reported by *Gordon et al*. [2001] south of Orkney Plateau, and limited relative to the interannual range in bottom potential temperature of 0.14°C documented by *Gordon et al*. [2010] in the same area.

A second hypothesis is that the lack of closure of the buoyancy budget of the abyssal Scotia Sea indicated by our work arises from methodological issues in the estimation of boundary mixing rates, and/or the spatially inhomogeneous and temporally intermittent nature of boundary mixing. Specifically, the empirical relationship between the Thorpe and Ozmidov scales upon which our estimates of boundary mixing rates hinge implicitly assumes that the vertical scale of turbulent overturns is free to evolve so that gravity balances the inertial forces of turbulence. This assumption is problematic in a boundary layer, as the overturning scale can be externally imposed. Another way of stating this is that the mixing efficiency in the relation (2) may well differ in the near-boundary region from its nominal value of $\Gamma=0.2$. As noted above, we have very little information on the extent to which our Orkney Passage analysis may be representative of other locations within the WSDW outflow's path along the southern Scotia Sea.

A third hypothesis is that the buoyancy budget of the southern Scotia Sea is closed in association with noninternal wave form drag related to flow separation and vortex shedding from complex two-dimensional topography in the interior basin. As a noninternal wave phenomenon, the associated buoyancy fluxes would not be addressed by the finescale parameterization (1). As a nonpropagating phenomenon, the related buoyancy fluxes would be closely tied to topography and potentially difficult to sample with free-

fall turbulence profilers. A common closure in the atmospheric literature [*Baines*, 1995] is to address this form drag with a quadratic drag law and $O(1)$ drag coefficient.

Finally, E. P. Abrahamsen *et al*. (in preparation) note a decadal-scale signature of decreasing volume of Lower WSDW in the Scotia Sea commencing near the turn of the century. Further considering the difference between the relatively large transport estimates in DOVETAIL and ALBATROSS and the smaller one in JR281, a reduced volume of Lower WSDW is consistent with a decreasing transport T^i and diapycnal transfers that are weakly dependent upon the average transport. If one were to argue that the area-averaged turbulent fluxes provided a negative feedback at a rate more than linearly proportional to T^i, the balance (3) would imply an increasing area A during the period of our data.

We surmise that resolving the abyssal Scotia Sea buoyancy budget problem may be contingent upon gaining a detailed quantitative understanding of boundary mixing mechanisms and associated temporal variability within Orkney Passage and along the basin's southern edge. To achieve a major advancement in our understanding of how mixing processes in the Orkney Passage contribute to the closure of the AABW control volume budget in the Scotia Sea (and, ultimately, how those processes mediate the wind's control of the AABW outflow through the passage), two new types of observations will be required. First, the detailed along-stream evolution of the thermohaline properties and velocity structure of the AABW outflow will have to be documented with a quasi-synoptic survey, to quantify the net transformations in the passage and identify the key mixing sites. Second, unambiguous identification of the processes underpinning AABW mixing in the passage will hinge on dedicated fine and microstructure measurements being obtained across the passage and over a sufficiently extensive period to resolve the major tidal frequencies.

Appendix A: Control Volume Budgets

Heywood et al. [2002] use approximate constructs for their control volume budgets that assume the fluid to be incompressible. We review the construction of such control volume statements to assess their sensitivity to that assumption.

The starting place for our concerns is the prescription for the diapycnal (dianeutral) velocity w^* [*McDougall*, 1987],

$$w^* = \frac{\partial K_\rho}{\partial z} + \frac{gK_\rho}{\overline{N^2}}(\alpha\bar{\theta}_{zz} - \beta\bar{S}_{zz}) - \frac{gK_\parallel}{\overline{N^2}}(T_b\nabla_n\bar{\theta}\cdot\nabla_n\bar{\theta} + C_b\nabla_n\bar{\theta}\cdot\nabla_n\bar{p}), \tag{A1}$$

in which K_ρ is the diapycnal diffusivity, N is the buoyancy frequency, and C_b and T_b are cabbeling and thermobaric coefficients related to nonlinearity in the equation of state. These are defined as

$$T_b = \frac{\partial\alpha}{\partial\theta} + 2\frac{\alpha}{\beta}\frac{\partial\alpha}{\partial S} - \frac{\alpha^2}{\beta^2}\frac{\partial\beta}{\partial S},$$

and

$$C_b = \frac{\partial\alpha}{\partial p} - \frac{\alpha}{\beta}\frac{\partial\beta}{\partial p}.$$

Here $\bar{\theta}$ might more properly be considered conservative temperature rather than potential temperature [*Klocker and McDougall*, 2010], but the distinction is immaterial for this application. Of concern are the effects of compressibility associated with isoneutral gradients of potential temperature and pressure in combination with large values of the cabbeling parameter at high pressure.

A control volume balance is constructed using the flux form of the conservation equations. Starting from the advective form of the conservation statement of a constituent C,

$$\partial_t C + \mathbf{u}\cdot\nabla C = 0, \tag{A2}$$

and incorporating mass conservation, i.e.,

$$\partial_t\rho + \mathbf{u}\cdot\nabla\rho + \nabla\cdot\mathbf{u} = 0, \tag{A3}$$

where ρ is *in situ* density, we obtain the flux form of the conservation equation of C, namely

$$\partial_t \rho C + \nabla \cdot \rho C \mathbf{u} = 0\,. \tag{A4}$$

The control volume balance is constructed by integrating (A4) and/or (A3) over that volume and invoking Green's theorem to change the volume integral into a surface integral. The typical situation is one in which dense fluid is provided to a basin through a choke point, which we label as an 'inlet' with superscript *i*, and potentially leaves via an outlet, with these contributions to the budget being advective in nature. These inlet/outlet advective fluxes are balanced by a combination of advective and eddy (turbulent) fluxes on an upper bounding surface. The eddy fluxes are treated by invoking a Reynolds decomposition into time mean and fluctuation. We first assume the bounding surface to be one of constant neutral density (γ^n=constant), so that the control volume version of the mass conservation equation (A3) is

$$\oint^i \bar{\rho}\, \bar{\mathbf{u}} \cdot d\mathbf{A} + \oint^\gamma \bar{\rho}\, \bar{\mathbf{u}} \cdot d\mathbf{A} = \oint^\gamma \overline{\mathbf{u}'\rho'} \cdot d\mathbf{A}, \tag{A5}$$

having neglected eddy fluxes at the inlet. An integral constraint on the transports

$$\begin{aligned} T^i &\equiv \oint^i \bar{\mathbf{u}} \cdot d\mathbf{A}; \quad \bar{\rho}^i = \oint^i \bar{\rho}\, \bar{\mathbf{u}} \cdot d\mathbf{A}/T^i, \\ T^\gamma &\equiv \oint^\gamma w^* dA; \quad \bar{\rho}^\gamma = \oint^\gamma \bar{\rho}\, \bar{\mathbf{u}} \cdot d\mathbf{A}/T^\gamma, \end{aligned} \tag{A6}$$

where w^* denotes the diapycnal velocity, can be easily derived. Representing advective *in situ* density fluxes in terms of transport-weighted means $\bar{\rho}^i$ and $\bar{\rho}^\gamma$ yields

$$\begin{aligned} \bar{\rho}^i T^i - \bar{\rho}^\gamma T^\gamma &= \oint^\gamma K_\rho \frac{\rho_o N^2}{g} dA, \\ \bar{\rho}^i T^i - (\bar{\rho}^i - \delta\bar{\rho})(T^i + \delta T) &\cong K_\rho \frac{\rho_o N^2}{g} A, \\ \frac{\delta T}{T^i} - \frac{\delta \rho}{\bar{\rho}^i} &\cong \frac{\rho_o K_\rho N^2 A}{g \bar{\rho}^i T^i}. \end{aligned} \tag{A7}$$

Even if the diapycnal diffusivity, K_ρ, is large, the right hand side of (A7) is small, specifically $O(10^{-5})$ for values in this work. Since $\delta\rho/\bar{\rho}^i$ is $O(10^{-3})$ or smaller, $\delta T/T^i$ is similarly $O(10^{-3})$ or smaller.

Thus, the advective contributions to w^* originating from nonlinearities in the equation of state [$\frac{gK_\parallel}{N^2} C_b \nabla_n \bar{\theta} \cdot \nabla_n \bar{p}$ in (A1)] will be cancelled by nearly equivalent amounts of diapycnal upwelling driven by turbulent motions, $\frac{\partial K_\rho}{\partial z} + \frac{gK_\rho}{N^2}(\alpha \bar{\theta}_{zz} - \beta \bar{S}_{zz})$.

With this integral constraint, the steady balance for *C* becomes

$$\oint \bar{\rho}\, \bar{C}\, \bar{\mathbf{u}} \cdot d\mathbf{A} \cong -\oint \bar{\rho}\, \overline{\mathbf{u}'C'} \cdot d\mathbf{A}. \tag{A8}$$

If variations of *in situ* density are neglected, consistent with approximating the flow as being incompressible [$\nabla \cdot \mathbf{u}$=0 in (A3)], then one arrives at the usual statement,

$$\oint \bar{C}\, \bar{\mathbf{u}} \cdot d\mathbf{A} \cong -\oint \overline{\mathbf{u}'C'} \cdot d\mathbf{A}, \tag{A9}$$

or, in a neutral coordinate,

$$\oint^i \bar{C}\, \bar{\mathbf{u}} \cdot d\mathbf{A} + \oint^\gamma \bar{C} w^* \cdot d\mathbf{A} = -\oint^\gamma \overline{\mathbf{u}'C'} \cdot d\mathbf{A}. \tag{A10}$$

Using (A7), one may write

$$\begin{aligned} T^i C^i &\equiv \oint^i \bar{C}\bar{\mathbf{u}} \cdot d\mathbf{A}, \\ T^\gamma C^\gamma &\equiv \oint^\gamma \bar{C} w^* \cdot d\mathbf{A} \cong w^* \oint^\gamma \bar{C} dA = T^i C^\gamma, \end{aligned} \tag{A11}$$

where the second (approximate) equality of the last line assumes that upwelling is evenly distributed over the upper bounding surface of the control volume. Here the contribution of the flux $\overline{\mathbf{u}'C'}$ to the integral is in the dianeutral direction, and hence is turbulent. Therefore,

$$T^i C^i - T^\gamma C^\gamma \cong K_\rho A \bar{C}_z \,. \tag{A12}$$

Acknowledgments
KLP gratefully acknowledges salary support from Woods Hole Oceanographic Institution bridge support funds. ACNG acknowledges the support of a Philip Leverhulme Prize. LJ and MPM were supported by the ANDREX project, funded by the U.K. National Environment Research Council (NE/E01366X/1). CTD and LADCP data utilized in this study can be obtained from the British Oceanographic Data Centre (BODC; www.bodc.ac.uk) and the Ocean Circulation Database (OCDB; www.awi.de).

References

Abrahamsen, P. (2011), *Cruise Report, RRS James Clark Ross JR252 & JR245C*, 30 pp., Br. Antarct. Surv., Cambridge, U. K. [Available at https://www.bodc.ac.uk/data/information_and_inventories/cruise_inventory/report/jr252.pdf.]

Aoki, S., S. R. Rintoul, S. Ushio, S. Watanabi, and N. L. Bindoff (2005), Freshening of the Adelie Land Bottom Water near 140° E, *Geophys. Res. Lett.*, *32*, L23601, doi:10.1029/2005GL024246.

Baines, P. B. (1995), *Topographic Effects in Stratified Flows*, pp. 482, Cambridge Univ. Press, Cambridge, U. K.

Baines, P. G. (1974), The generation of internal tides over steep continental slopes, *Philos. Trans. R. Soc. London A*, *277*, 27–58.

Brink, K. H., and S. J. Lentz (2010a), Buoyancy arrest and bottom Ekman transport, part I: Steady flow, *J. Phys. Oceanogr.*, *40*, 621–635.

Brink, K. H., and S. J. Lentz (2010b), Buoyancy arrest and bottom Ekman transport, part II: Oscillating flow, *J. Phys. Oceanogr.*, *40*, 636–654.

Dillon, T. M. (1982), Vertical overturns: A comparison of Thorpe and Ozmidov length scales, *J. Geophys. Res.*, *87*, 9601–9613.

Fahrbach, E., M. Hoppema, G. Rohardt, M. Schröder, and A. Wisotzki (2004), Decadal-scale variations of water mass properties in the deep Weddell Sea, *Ocean Dyn.*, *54*, 77–91.

Fahrbach, E., M. Hoppema, G. Rohardt, O. Boebel, O. Klatt, and A. Wisotzki (2011), Warming of deep and abyssal water masses along the Greenwich meridian on decadal time scales: The Weddell gyre as a heat buffer, *Deep-Sea Res. II*, *58*, 2509–2523.

Ferron, B., H. Mercier, K. Speer, A. Gargett, and K. L. Polzin (1998), Mixing in the Romanche Fracture Zone, *J. Phys. Oceanogr.*, *28*(10), 1929–1945.

Gargett, A. and T. Garner (2008), Determining Thorpe scales from ship-lowered CTD density profiles, *J. Atmos. Oceanic Technol.*, *25*, 1657–1670.

Gordon, A. L., M. Visbeck, and B. Huber (2001), Export of Weddell Sea deep and bottom water, *J. Geophys. Res.*, *106*, 9005–9017.

Gordon, A. L., B. Huber D. McKee, and M. Visbeck (2010), A seasonal cycle in the export of bottom water from the Weddell Sea, *Nat. Geosci.*, *3*, 551–556, doi:10.1038/ngeo916.

Heywood, K. J., A. C. Naveira Garabato, and D. P. Stevens (2002), High mixing rates in the abyssal Southern Ocean, *Nature*, *415*, 1011–1014.

Iudicone, D., G. Madec, and T. J. McDougall (2008), Watermass transformations in a neutral density framework and the key role of light penetration, *J. Phys. Oceanogr.*, *38*, 1357–1376.

Jacobs, S. S. and C. F. Giulivi (2010), Large mutidecadal salinity trends near the Pacific-Antarctic continental margin, *J. Clim.*, *23*, 4508–4524.

Johnson, G. C., and S. C. Doney (2006), Recent western South Atlantic bottom water warming, *Geophys. Res. Lett.*, *33*, L14614, doi:10.1029/2006GL026769.

Jullion, L., S. C. jones, A. C. Naveira Garabato, and M. P. Meredith (2010), Wind-controlled export of Antarctic Bottom Water from the Weddell Sea, *Geophys. Res. Lett.*, *37*, L09609, doi:10.1029/2010GL042822.

Jullion, L., A. C. Naveira Garabato, M. P. Meredith, P. R. Holland, P. Courtois, and B. A. King (2013), Decadal freshening of the Antarctic Bottom Water exported from the Weddell Sea, *J. Clim.*, *26*, 8111–8125.

Jullion, L., et al. (2014), The contribution of the Weddell Gyre to the lower limb of the global overturning circulation, *J. Geophys. Res. Oceans*, *119*, 3357–3387, doi:10.1002/2013JC009725.

Klocker, A. and T. J. McDougall (2010), Influence of the nonlinear equation of state on global estimates of dianeutral advection and diffusion, *J. Phys. Oceanogr.*, *40*, 1690–1709.

MacCready, P., and P. B. Rhines (1993), Slippery bottom boundary layers on a slope, *J. Phys. Oceanogr.*, *23*, 5–22.

Martinson, D., and R. Iannuzzi (2003), Spatial/temporal patterns in Weddell Gyre characteristics and their relationship to global climate, *J. Geophys. Res.*, *108*(C4), 8083, doi:10.1029/2000JC000538.

McDougall, T. J. (1987), Thermobaricity, cabbeling, and water-mass conversion, *J. Geophys. Res.*, *92*, 5448–5464.

Meredith, M. (2010), *Cruise Report, RRS James Clark Ross JR235/236/239*, 147 pp., Br. Antarct. Surv., Cambridge, U. K. [Available at https://www.bodc.ac.uk/data/information_and_inventories/cruise_inventory/report/jr235_236_239.pdf.]

Meredith, M. P., A. C. N. Garabato, A. L. Gordon, and G. C. Johnson (2008), Evolution of the deep and bottom waters of the Scotia Sea, Southern Ocean, during 1995–2005, *J. Clim.*, *21*, 3327–3343.

Meredith, M. P., et al. (2011a), Sustained monitoring of the Southern Ocean at Drake Passage: Past achievements and future priorities, *Rev. Geophys.*, *49*, RG4005, doi:10.1029/2010RG000348.

Meredith, M. P., A. L. Gordon, A. C. Naveira Garabato, E. P. Abrahamsen, B. A. Huber, L. Jullion H. J. Venables (2011b), Synchronous intensification and warming of Antarctic Bottom Water outflow from the Weddell Gyre. *Geophys. Res. Lett.*, *38*, L03603, doi:10.1029/2010GL046265.

Meredith, M. P., P. J. Brown, A. C. Naveira Garabato, L. Jullion, H. J. Venables, and M.-J. Messias (2013), Dense bottom layers in the Scotia Sea, Southern Ocean: Creation, lifespan and destruction, *Geophys. Res. Lett.*, *40*, 933–936, doi:10.1002/grl.50260.

Molemaker, M. J., J. C. McWilliams, and I. Yavneh (2005), Baroclinic instability and loss of balance, *J. Phys. Oceanogr.*, *35*, 1505–1517.

Naveira Garabato, A. C., E. L. McDonagh, D. P. Stevens, K. J. Heywood, and R. J. Sanders (2002), On the export of Antarctic bottom water from the Weddell Sea, *Deep Sea Res., Part II*, *49*, 4715–4742.

Naveira Garabato, A. C., K. L. Polzin, B. A. King, K. J. Heywood, and M. Visbeck (2004), Widespread intense turbulent mixing in the Southern Ocean, *Science*, *303*, 210–213.

Naveira Garabato, A. C., R. Ferrari, and K. L. Polzin (2011), Eddy stirring in the Southern Ocean, *J. Geophys. Res.*, *116*, C09019, doi:10.1029/2010JC006818.

Naveira Garabato, A. C., A. P. Williams, and S. Bacon (2014), The three-dimensional overturning of the Southern Ocean during the WOCE era, *Prog. Oceanogr.*, *120*, 41–78.

Nicholls, K., P. Abrahamsen, M. Biuw, L. Böhm and P. Mele (2007), *Report for Cruises ES031, ES038 and ES048 ACES-FOCAS Cruise to the southern Weddell Sea, RRS Ernest Shackleton*, 50 pp., Br. Antarct. Surv., Cambridge, U. K. [Available at https://www.bodc.ac.uk/data/information_and_inventories/cruise_inventory/report/ernest_shackleton031-038-048.pdf.]

Nicholls, K., I. Fer, C. Griffiths, B. Huber, and P. Robinson (2009), *Report for Cruise ES033 Second ACES-FOCAS cruise to the southern Weddell Sea, RRS Ernest Shackleton*, 57 pp., Br. Antarct. Surv., Cambridge, U. K. [Available at https://www.bodc.ac.uk/data/information_and_inventories/cruise_inventory/report/ernest_shackleton033.pdf.]

Nicholls, K. W., S. Østerhus, K. Makinson, T. Gammelsrød, and E. Fahrbach (2009), Ice-ocean processes over the continental shelf of the southern Weddell Sea, Antarctica: A review, *Rev. Geophys.*, *47*, RG3003, doi:10.1029/2007RG000250.

Padman, L., S. Howard, and R. Muench (2006), Internal tide generation along the South Scotia Ridge, *Deep Sea Res., Part II*, *53*, 157–171.

Polzin, K. L., A. C. Naveira Garabato, T. N. Huussen, B. M. Sloyan, and S. N. Waterman (2014), Finescale parameterizations of turbulent dissipation, *J. Geophys. Res. Oceans*, *119*, 1383–1419, doi:10.1002/2013JC0089789.

Purkey, S. G., and G. C. Johnson (2010), Warming of global abyssal and deep Southern Ocean waters between the 1990s and 2000s: Contributions to global heat and sea level rise budgets, *J. Clim.*, *23*, 6336–6351.

Ralph, E. A., and P. P. Niiler (1999), Wind-driven currents in the Tropical Pacific, *J. Phys. Oceanogr.*, *29*, 2121–2129.

Rintoul, S. R. (2007), Rapid freshening of Antarctic bottom water formed in the Indian and Pacific oceans, *Geophys. Res. Lett.*, *34*, L06606, doi:10.1029/2006GL028550.

Rye, C. D., A. C. Naveira Garabato, P. R. Holland, M. P. Meredith, A. J. George Nurser, C. W. Hughes, A. C. Coward, and D. J. Webb (2014), Rapid sea-level rise along the Antarctic margins in response to increased glacial discharge, *Nat. Geosci.*, *7*, 732–735, doi:10.1038/ngeo2230.

Schröder, M., H. H. Hellmer, and J. M. Absy (2002), On the near bottom variability in the northwestern Weddell Sea, *Deep Sea Res., Part II*, *49*, 4767–4790.

Sheen, K. L., et al. (2013), Rates and mechanisms of turbulent dissipation and mixing in the Southern Ocean: Results from the Diapycnal and Isopycnal Mixing Experiment in the Southern Ocean (DIMES), *J. Geophys. Res. Oceans*, *118*, 2774–2792, doi:10.1002/jgrc.20217.

Sheen, K. L., et al. (2014), Southern Ocean abyssal mixing on climatic timescales, *Nat. Geosci.*, *7*, 577–582, doi:10.1038/ngeo2200.

Thorpe, S. A. (1977), Turbulence and mixing in a Scottish loch, *Philos. Trans. R. Soc. London A*, *286*, 125–181.

Toggweiller, J. R., J. L. Russell, and S. R. Carson (2006), Midlatitude westerlies, atmospheric CO_2, and climate change during ice ages, *Paleoceanography*, *21*, PA2005, doi:10.1029/2005PA001154.

Trowbridge, J. H., and S. J. Lentz (1991), Asymmetric behavior of an oceanic boundary layer above a sloping bottom, *J. Phys. Oceanogr.*, *21*, 1171–1185.

Tulloch, R., R. Ferrari, O. Jahn, A. Klocker, J. LaCasce, J. R. Ledwell, J. Marchall, M.-J. Messias, K. Speer and A. Watson (2014), Direct estiamte of lateral eddy diffusivity upstream of Drake Passage, *J. Phys. Oceanogr.*, *44*, 2593–2616.

Waterman, S. N., K. L. Polzin, A. C. Naveira Garabato, K. L. Sheen, and A. Forryan (2014), Suppression of internal wave breaking in the Antarctic Circumpolar Current near topography, *J. Phys. Oceanogr.*, *44*, 1466–1492.